THE
EMBO
JOURNAL

Structural basis and kinetics of inter- and intramolecular disulfide exchange in the redox catalyst DsbD

Anna Rozhkova[1,4],
Christian U Stirnimann[2,4], Patrick Frei[1],
Ulla Grauschopf[1], René Brunisholz[3],
Markus G Grütter[2], Guido Capitani[2,*]
and Rudi Glockshuber[1,*]

[1]Institut für Molekularbiologie und Biophysik, Eidgenössische Technische Hochschule Hönggerberg, Zürich, Switzerland, [2]Biochemisches Institut, Universität Zürich, Winterthurerstrasse, Zürich, Switzerland and [3]Protein-Servicelabor, Departement Biologie, Eidgenössische Technische Hochschule Hönggerberg, Zürich, Switzerland

DsbD from *Escherichia coli* catalyzes the transport of electrons from cytoplasmic thioredoxin to the periplasmic disulfide isomerase DsbC. DsbD contains two periplasmically oriented domains at the N- and C-terminus (nDsbD and cDsbD) that are connected by a central transmembrane (TM) domain. Each domain contains a pair of cysteines that are essential for catalysis. Here, we show that Cys109 and Cys461 form a transient interdomain disulfide bond between nDsbD and cDsbD in the reaction cycle of DsbD. We solved the crystal structure of this catalytic intermediate at 2.85 Å resolution, which revealed large relative domain movements in DsbD as a consequence of a strong overlap between the surface areas of nDsbD that interact with DsbC and cDsbD. In addition, we have measured the kinetics of all functional and nonfunctional disulfide exchange reactions between redox-active, periplasmic proteins and protein domains from the oxidative DsbA/B and the reductive DsbC/D pathway. We show that both pathways are separated by large kinetic barriers for nonfunctional disulfide exchange between components from different pathways.

*Corresponding authors. Rudi Glockshuber, Institut für Molekularbiologie und Biophysik, Eidgenössische Technische Hochschule Hönggerberg, CH-8093 Zürich, Switzerland. Tel.: +41 1 633 6819; Fax: +41 1 633 1036; E-mail: rudi@mol.biol.ethz.ch or Guido Capitani, Biochemisches Institut, Universität Zürich, Winterthurerstrasse 190, CH-8057 Zürich, Switzerland. Tel.: +41 1 635 5587; Fax: +41 1 635 6834; E-mail: capitani@bioc.unizh.ch
[4]These authors contributed equally to this work

Introduction

Disulfide bonds are a typical post-translational modification of secretory proteins. In bacteria, disulfide bond formation occurs in the oxidizing environment of the periplasm and is catalyzed by redox enzymes of the Dsb family. Two types of reactions are primarily required for correct formation of disulfide bonds in proteins with multiple disulfide bonds: disulfide bond formation and disulfide bond isomerization (Ritz and Beckwith, 2001; Collet and Bardwell, 2002; Hiniker and Bardwell, 2003). Each of these reactions is linked with an independent electron transfer pathway in *Escherichia coli*. The pathway of disulfide bond formation involves the oxidation of reduced, newly translocated proteins by the periplasmic dithiol oxidase DsbA. DsbA belongs to the thioredoxin family and has a very reactive disulfide bond (active site: Cys-Pro-His-Cys), which is transferred randomly and extremely rapidly to reduced polypeptide substrates by disulfide exchange (Wunderlich *et al*, 1993; Zapun and Creighton, 1994; Darby and Creighton, 1995). Polypeptide oxidation generates reduced DsbA, which is reoxidized by ubiquinone from the respiratory chain, a two-electron transfer reaction catalyzed by the inner membrane protein DsbB (Bardwell *et al*, 1993; Dailey and Berg, 1993; Bader *et al*, 2000; Grauschopf *et al*, 2003). The reduced quinone (ubiquinol) is then reoxidized by molecular oxygen via terminal cytochrome oxidases (Bader *et al*, 1999; Kobayashi and Ito, 1999). The pathway of disulfide isomerization copes with wrong disulfide bonds randomly introduced by DsbA. The disulfide isomerase DsbC, a homodimeric, periplasmic protein with the active site Cys-Gly-Tyr-Cys, attacks wrong disulfide bonds in scrambled polypeptide substrates, and catalyzes their rearrangement to the native conformation (Missiakas *et al*, 1994; Zapun *et al*, 1995; McCarthy *et al*, 2000; Maskos *et al*, 2003). Consequently, for being active as a catalyst, DsbC has to be kept in a reduced state in an otherwise oxidizing cellular compartment. This is achieved through a specific electron transfer cascade in which two electrons from cytoplasmic NADPH flow to cytoplasmic thioredoxin, then to the inner membrane protein DsbD, and then to periplasmic DsbC (Rietsch *et al*, 1997; Chung *et al*, 2000; Krupp *et al*, 2001).

DsbD consists of 546 amino acids and is composed of a periplasmically oriented, N-terminal domain with immuno-globulin-like fold (nDsbD), a central transmembrane (TM) domain predicted to be composed of eight TM helices, and a C-terminal domain with thioredoxin fold (cDsbD) that is again oriented toward the periplasm (Gordon *et al*, 2000). Each of the three domains contains one pair of invariant cysteines that are essential for electron transport from thioredoxin to DsbC (Stewart *et al*, 1999). It was hence postulated that the catalytic mechanism of DsbD is exclusively based on disulfide exchange reactions between DsbD and its substrate proteins, and intramolecular disulfide interchange between
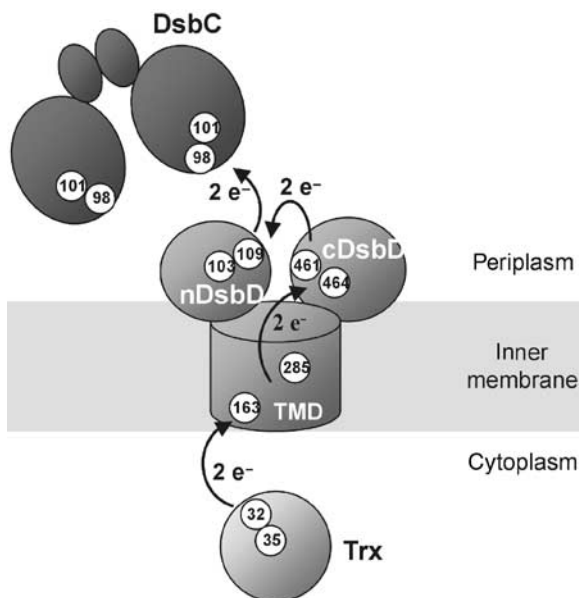
Figure 1 Proposed electron flow from reduced thioredoxin in the cytoplasm to oxidized, homodimeric DsbC in the periplasm via DsbD. According to this mechanism, electron transport occurs exclusively through intermolecular and intramolecular disulfide exchange. DsbD consists of an N-terminal domain (nDsbD, residues 1–143) and a C-terminal domain (cDsbD; residues 419–546), which are oriented toward the periplasm, and a central TM domain (residues 144–418). Numbered circles represent essential cysteine residues in the respective protein.

the three DsbD domains (Goldstone *et al*, 2001; Krupp *et al*, 2001; Collet *et al*, 2002; Katzen and Beckwith, 2003). According to this model, oxidizing equivalents are transferred from oxidized DsbC to the Cys103/Cys109 pair of nDsbD, then to Cys461/Cys464 of the cDsbD, followed by oxidation of the Cys163/Cys285 pair of the TM domain, which eventually oxidizes thioredoxin in the cytoplasm (Figure 1). Besides DsbC, the proteins DsbG and CcmG (DsbE) are further known *in vivo* substrates of DsbD that are kept in a reduced state in the periplasm. DsbG is a homodimeric homolog of DsbC (26% sequence identity) of unknown function (Andersen *et al*, 1997; van Straaten *et al*, 1998; Bessette *et al*, 1999), and CcmG is a membrane-anchored enzyme with thioredoxin fold that is required for cytochrome *c* biogenesis (Reid *et al*, 2001).

Available structural information on DsbD includes the X-ray structure of oxidized nDsbD and the X-ray structure of the mixed disulfide between the Cys103Ala variant of nDsbD and the Cys101Ser variant of DsbC (Goulding *et al*, 2002; Haebel *et al*, 2002). In addition, a crystal structure of oxidized cDsbD has been reported (Kim *et al*, 2003). Importantly, the nDsbD-SS-DsbC complex exhibits a stoichiometry of one nDsbD monomer per DsbC homodimer. This is due to the fact that nDsbD does not only interact with residues around the active site disulfide of a DsbC subunit, but forms specific, additional contacts with the second subunit in the DsbC dimer that prevent binding of a second nDsbD equivalent in a symmetry-related manner.

Several aspects of the above model for the DsbD cycle raise questions regarding the structure of DsbD. In particular, it is not obvious how two cysteines in the TM domain should suffice to transport electrons over a distance of about 60 Å (membrane thickness) via a 'disulfide ladder' from the cytoplasm to the periplasm. In addition, the cysteine residues that
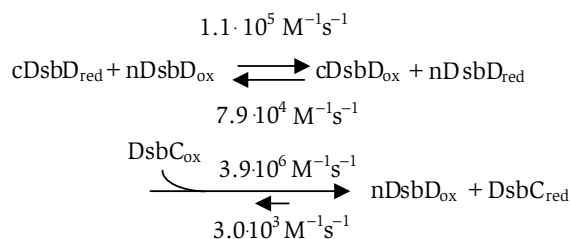
are involved in intramolecular disulfide interchange between the three domains in DsbD have not yet been identified. Here, we show that Cys109 and Cys461 mediate disulfide interchange between nDsbD and cDsbD. In addition, we solved the crystal structure of the kinetically stabilized mixed disulfide between both domains. The mixed disulfide complex represents a trapped intermediate in the catalytic cycle of DsbD, and reveals that large domain movements must occur during catalysis of electron transfer. Moreover, we demonstrate that both the reduction of DsbC by nDsbD, and disulfide interchange between nDsbD and cDsbD are very rapid processes. Finally, we show that the DsbA/B and DsbC/D redox systems are separated by large kinetic barriers that appear exclusively caused by steric block of disulfide exchange.

Results

Physical properties of the isolated periplasmic domains nDsbD and cDsbD

We expressed and purified the isolated periplasmic domains of DsbD, nDsbD (residues 1–143 of mature DsbD), and a C-terminally $(His)_6$-tagged variant of cDsbD (residues 419–546). To test the intrinsic reactivity of the individual domains, we analyzed the kinetics of electron transfer from reduced cDsbD via oxidized nDsbD to oxidized DsbC by reversed-phase HPLC separation of acid-quenched reactions products (Figure 2A). We found that the overall reaction is very rapid at pH 7.0 and 25°C, and yields reduced DsbC, oxidized nDsbD, and oxidized cDsbD within about 500 s when low initial concentrations of 0.25 μM were used for all proteins (monomer concentration in the case of DsbC). No mixed disulfides between nDsbD and DsbC, or nDsbD and cDsbC were detected. This indicates that these mixed disulfides are kinetically unstable and dissociate very rapidly by intramolecular disulfide exchange. As a control, we showed that the reverse reaction is not observed (Figure 2B). In addition, we measured the redox potentials of cDsbD, nDsbD, and DsbC at pH 7.0 and 25°C in identical buffer conditions, and obtained values of −0.235, −0.232, and −0.140 V, respectively (Figure 2F). The redox potential of DsbC and the practically identical potentials of cDsbD and nDsbD are in good agreement with previous measurements (Zapun *et al*, 1995; Collet *et al*, 2002) and confirm that complete electron transfer from cDsbD to DsbC via nDsbD is thermodynamically driven.

We next measured the individual microscopic rate constants of electron transfer from cDsbD to nDsbD, and from nDsbD to DsbC. Figures 2C and D show that reduction of DsbC by nDsbD is extremely rapid (3.9×10^6 M^{-1} s^{-1}), while intermolecular disulfide exchange between cDsbD and nDsbD is more than one order of magnitude slower. Thus, electron transfer between cDsbD and nDsbD is rate-limiting for the overall *in vitro* reaction according to the following scheme.
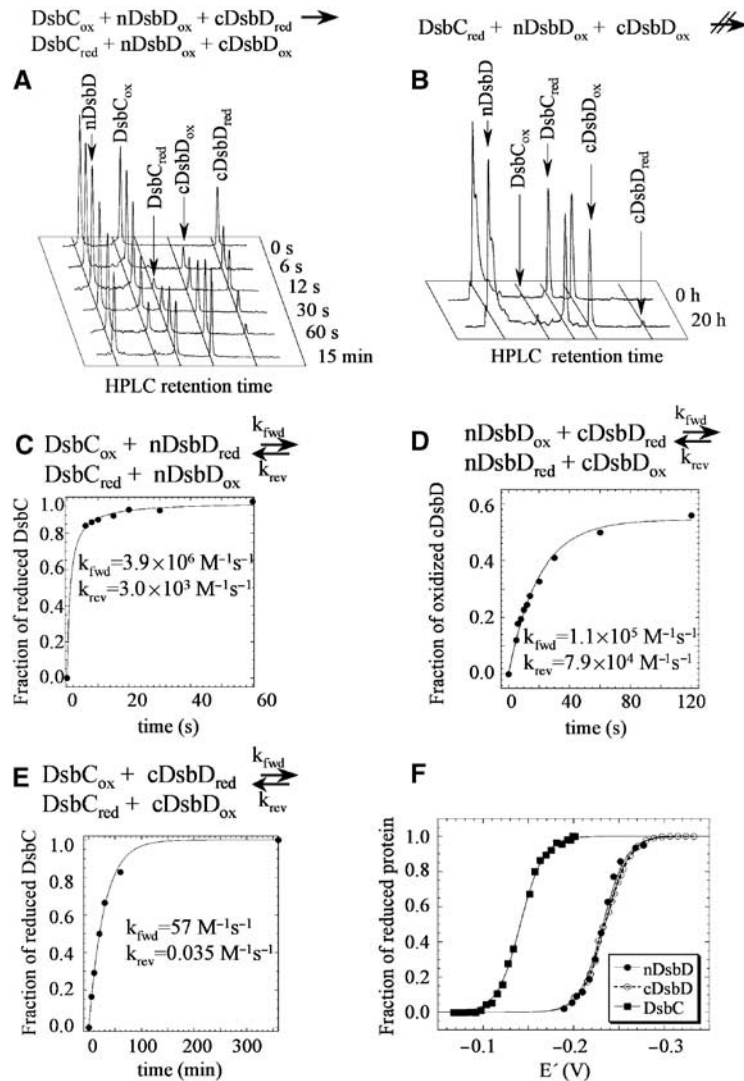
$$1.1 \cdot 10^5 \text{ M}^{-1}\text{s}^{-1}$$

$$\text{cDsbD}_{red} + \text{nDsbD}_{ox} \rightleftharpoons \text{cDsbD}_{ox} + \text{nDsbD}_{red}$$

$$7.9 \cdot 10^4 \text{ M}^{-1}\text{s}^{-1}$$

$$\text{DsbC}_{ox} \xrightarrow{3.9 \cdot 10^6 \text{ M}^{-1}\text{s}^{-1}} \text{nDsbD}_{ox} + \text{DsbC}_{red}$$

$$3.0 \cdot 10^3 \text{ M}^{-1}\text{s}^{-1}$$

Figure 2 Kinetics of electron transport from cDsbD via nDsbD to DsbC at 25°C and pH 7.0. The reactions were acid-quenched after different incubation times, and products were separated on a C_{18} reverse-phase HPLC column. (**A**) $DsbC_{ox}$, $nDsbD_{ox}$, and $cDsbD_{red}$ (0.25 µM each) were mixed at a 1:1:1 ratio. Note that $nDsbD_{ox}$ and $nDsbD_{red}$ cannot be separated under these conditions. (**B**) No electron flow from $DsbC_{red}$ to $cDsbD_{ox}$ or $nDsbD_{ox}$ is observed. (**C**) Reduction of $DsbC_{ox}$ by $nDsbD_{red}$. Initial protein concentrations were 0.25 µM. The solid line corresponds to a second-order fit, with a rate constant of $3.9 \times 10^6 \, M^{-1} \, s^{-1}$. The rate constant of the reverse reaction ($3.0 \times 10^3 \, M^{-1} \, s^{-1}$) was deduced from the equilibrium constant of 1300 for the reduction of DsbC by nDsbD. (**D**) Disulfide exchange kinetics between isolated nDsbD and cDsbD. $nDsbD_{red}$ and $cDsbD_{ox}$ (0.25 µM each) were mixed, and the attainment of the equilibrium was fitted according to second-order kinetics for the forward and the reverse reaction with the program *Berkeley Madonna*. The obtained equilibrium constant of 1.4 agrees well with the calculated equilibrium constant of 1.3 from the redox potential measurements (see panel F). The fit (solid line) yielded rate constants of 1.1×10^5 and $7.9 \times 10^4 \, M^{-1} \, s^{-1}$ for the forward and reverse reactions, respectively. (**E**) Direct reduction of $DsbC_{ox}$ by $cDsbD_{red}$ in the absence of nDsbD. The reaction was performed under pseudo-first-order conditions, with initial concentrations of 1 µM for $DsbC_{ox}$ (monomer) and 10 µM for $cDsbD_{red}$. The fit (solid line) yields a rate constant of $57 \, M^{-1} \, s^{-1}$. The rate constant for the reverse reaction was calculated from the equilibrium constant (1600) for the reduction of DsbC by cDsbD. (**F**) Determination of the redox potentials of nDsbD, cDsbD, and DsbC at pH 7.0 and 25°C by equilibration of proteins with thiol-disulfide redox buffers (see Materials and methods for details). All concentrations of DsbC refer to the DsbC monomer.

However, disulfide exchange between nDsbD and cDsbD is most likely not rate-limiting for the reaction cycle of intact DsbD, where nDsbD and cDsbD are covalently linked and thus expected to have very high effective concentrations. As an additional control, we showed that direct reduction of DsbC by cDsbD is almost five orders of magnitude slower ($k_2 = 57 \, M^{-1} \, s^{-1}$) compared to the reduction by nDsbD (Figures 2E and 6). This result explains why both periplasmic domains of DsbD are required for shuffling electrons from the TM domain of DsbD to DsbC.

Cys109 and Cys461 form a mixed disulfide between nDsbD and cDsbD

To identify the cysteine residues that form a transient mixed disulfide between nDsbD and cDsbD in the DsbD reaction cycle, we purified the single-cysteine variants Cys103Ser and Cys109Ser of nDsbD, and Cys461Ser and Cys464Ser of cDsbD. Free thiol groups in the purified proteins were quantified with Ellman's assay both at the level of the native and denatured states. Table I shows that only Cys109 of nDsbD and Cys461 of cDsbD are reactive and solvent accessible, while Cys103

and Cys464 are buried in the folded domains. Consequently, disulfide exchange between nDsbD and cDsbD can only occur via a transient disulfide bond between Cys109 and Cys461. To prepare a kinetically stable mixed disulfide between nDsbD and cDsbD, we first synthesized the activated mixed disulfide between nDsbD-C103S and thionitrobenzoic acid by incubation of nDsbD-C103S with excess of Ellman's reagent. The activated mixed disulfide was then purified and mixed with equimolar amounts of the variant cDsbD-C464S, which resulted in almost quantitative formation of the mixed disulfide between nDsbD-C103S and cDsbD-C464S (Supplementary Figure S1). The reaction product was purified to homogeneity by chromatography on Ni-NTA agarose and gel filtration, concentrated to 40 mg/ml, and crystallized.

Structure determination of the mixed disulfide between nDsbD and cDsbD

The X-ray structure of the mixed disulfide between nDsbD and cDsbD (termed nDsbD-SS-cDsbD in the following) was

Table 1 Accessible thiols in single-cysteine variants of nDsbD and cDsbD

Domain variant	Free thiols/polypeptide	
	Denatured[a]	Native
nDsbD-C103S	0.98	1.04
nDsbD-C109S	1.02	0.07
cDsbD-C461S	1.04	0.12
cDsbD-C464S	1.07	0.98

[a]In the presence of 6 M guanidinium chloride.

solved at a resolution of 2.85 Å (PDB entry 1SE1). The crystals belong to space group C2 and contain three nDsbD-SS-cDsbD complexes (A–C) per asymmetric unit. The structure reveals in full detail how the N-terminal immunoglobulin-like domain of DsbD interacts with the C-terminal thioredoxin-like domain.

The final electron density map is well defined throughout the structure, which was refined to an *R*-factor of 0.224 and a free *R*-factor of 0.284 (Table II). The Ramachandran plot statistics is very good (Table II) with only one residue (Asp79 from nDsbD) in the disallowed region. The electron density of Asp79 is well defined and was found to be identical in the structure of noncomplexed nDsbD (Goulding *et al* (2002), PDB entry 1L6P (1.65 Å), Haebel *et al* (2002), PDB entry 1JPE (1.9 Å)) and for the complex between nDsbD and DsbC (nDsbD-SS-DsbC, Haebel *et al* (2002), PDB entry 1JZD (2.3 Å)), respectively.

The average *B*-factor for the final nDsbD-SS-cDsbD model is 38.4 Å² , which compares with a Wilson *B*-factor of 68.8 Å² for the data and with an average *B*-factor of 43.3 Å² for the structure of nDsbD-SS-DsbC (PDB entry 1JZD).

Overall structure of nDsbD-SS-cDsbD

nDsbD possesses an immunoglobulin-like fold (Goulding *et al*, 2002), and cDsbD a thioredoxin-like fold (Kim *et al*, 2003). Each nDsbD-SS-cDsbD complex has dimensions of about 34 Å × 43 Å × 75 Å (Figure 3A). Comparison of the nDsbD-SS-DsbC complex with nDsbD-SS-cDsbD reveals similarities and differences in the binding mode and interfaces. As Cys109 of nDsbD forms a mixed disulfide with the solvent-exposed, nucleophilic cysteine of its reaction partner in both

Table 2 Crystallographic data and refinement statistics

Data collection

Radiation source	SLS Villigen, CH beamline X06SA
Wavelength (Å)	0.7514
Space group	C2
Unit cell (Å³)	$188.5 \times 52.6 \times 107.9$, $\beta = 100.4°$
Resolution range (Å)	20–2.85
No. of reflections	109 492
No. of unique reflections	24 676
Completeness (%)	99.3 (97.3)[a]
R_{sym}	8.0 (36.2)[a]
Average I/σ	16.1 (3.6)[a]
Redundancy	4.4 (3.3)[a]

Refinement statistics

Resolution (Å)	20–2.85			
No. of reflections (test)	24 336 (707)			
No. of atoms	Complex A	Complex B	Complex C	Total
nDsbD	979	915	927	2821
CDsbD	1000	931	922	2853
Water molecules				284
R-factor	0.224 (0.349)[b]			
Free *R*-factor	0.284 (0.443)[b]			
R.m.s.d. bonds (Å)	0.0076			
R.m.s.d. angles (deg)	1.24			
Average *B*-factor (Å²)	38.4			

Ramachandran plot regions (%)

Most favored	89.7%
Additional allowed	9.2%
Generously allowed	0.6%
Disallowed region	0.5%

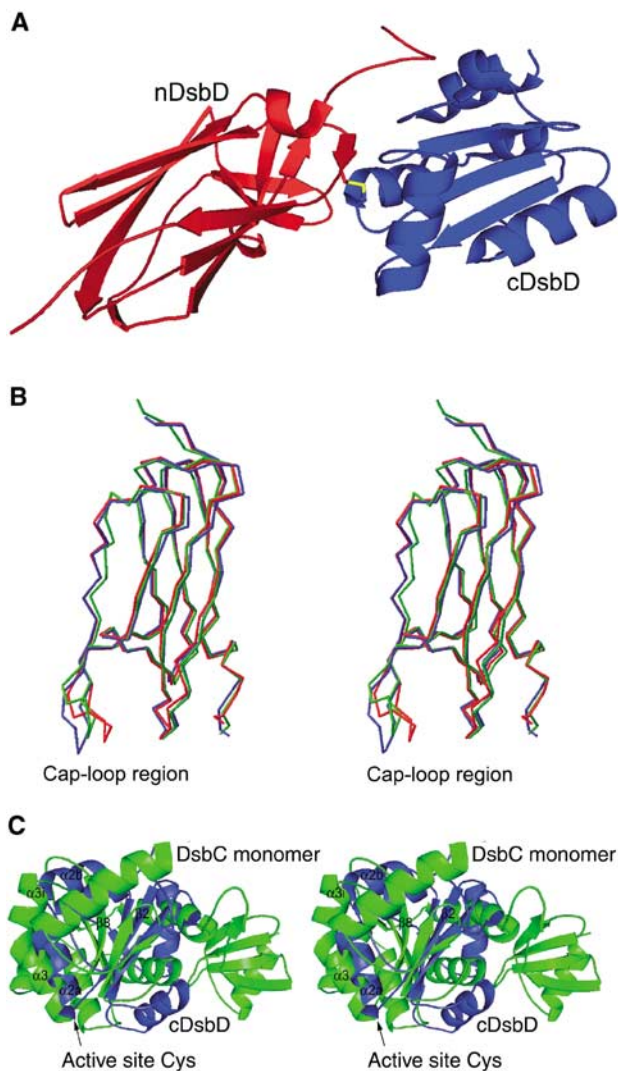[a]Last shell: 2.85–2.95 Å.
[b]Last shell: 2.85–3.03 Å.

Figure 3 (**A**) Ribbon diagram of the structure of the nDsbD-SS-cDsbD mixed disulfide. The structure of nDsbD (red) comprises residues 1–125, and that of cDsbD (blue) residues 426–545 (complex B). The disulfide bond between Cys109 and Cys461 is depicted in yellow. (**B**) Superposition of the C^α-traces of nDsbD from the nDsbD-SS-DsbC complex (1JZD, green) and nDsbD from nDsbD-SS-cDsbD complex (complex B, blue) onto that of monomeric nDsbD (1L6P, red) shows different conformations of the Cap-loop region (residues 68–72). (**C**) Stereo picture showing differences in the orientation of cDsbD (blue) and DsbC (green) in the complex with nDsbD (not shown), based on superposition of nDsbD from nDsbD-SS-DsbC (1JZD) onto nDsbD from the nDsbD-SS-cDsbD complex. The arrow indicates the approximate position of the active site cysteines for both complexes.

complexes, the contact areas of nDsbD for binding of cDsbD and DsbC overlap. Cys109 in isolated oxidized nDsbD is shielded by the so-called Cap-loop region (segment Asp68–Gly72) (Goulding *et al*, 2002). As reported for the nDsbD-SS-DsbC complex (Haebel *et al*, 2002), Cys109 of nDsbD becomes accessible in nDsbD-SS-cDsbD due to a conformational switch of that region. The Cap-loop region is in a more open conformation in nDsbD-SS-cDsbD than in the nDsbD-SS-DsbC complex (Figure 3B). Crystal contacts between nDsbD-SS-nDsbD complexes A and C may contribute to this difference. In the case of complex B, the Cap-loop

region is involved only in a weak crystal contact with complex A through a hydrogen bond. Electron density for residues Phe70 and Tyr71 (side chain only) in complex B is poorly defined, indicating that the Cap-loop region is flexible.

Kim *et al* (2003) previously modelled the nDsbD-SS-cDsbD complex using the nDsbD-SS-DsbC structure (Haebel *et al*, 2002) as a template. However, the orientation of cDsbD relative to nDsbD in the experimental structure of nDsbD-SS-cDsbD differs from this model (Figure 3C). For example, helix α2a and strand β2 of cDsbD have a different orientation (an angle of ∼20°) than the corresponding helix α3 and strand β8 of DsbC in the model.

The three copies of the nDsbD domain in the asymmetric unit also exhibit differences around the N-termini due to crystal contacts. In complex A, electron density is visible for residues Gly1 to Ala5, then there is a gap until Gln10. In complex B, the entire N-terminal region has well-defined electron density, whereas no clear electron density is discernible before Ser9 in complex C. These N-terminal residues in complexes A and B adopt different conformations, which again appear to be caused by crystal contacts.

A surface representation of nDsbD-SS-cDsbD shows a relatively planar region between the C-terminus of nDsbD and the N-terminus of cDsbD, which is supposed to be oriented towards the surface of the membrane (Supplementary Figure S2). The TM domain of DsbD consists of eight predicted TM helices (Stewart *et al*, 1999; Chung *et al*, 2000; Gordon *et al*, 2000). Recently, Katzen and Beckwith (2003) showed that Cys163 from the first predicted TM helix 1 can form a disulfide bridge with Cys285 from the fourth TM helix, and proposed a model for the TM domain in which helices 1 and 8 are adjacent. This model would require long linker segments to connect the TM domain with the crystallographically observed C-terminus of nDsbD and N-terminus of cDsbD, which are approximately 60 Å apart. The 20 residues separating the last observed residue of nDsbD from the first predicted residue of TM helix 1, and the 15 residues between the last residue of the predicted TM helix 8 and the first observed residue of cDsbD may span this distance. Comparison of the structure of nDsbD-SS-cDsbD with that of nDsbD-SS-DsbC suggests that a large translation of nDsbD away from cDsbD is required to allow disulfide exchange of nDsbD in the context of full-length DsbD with the active site of DsbC. In addition, there may be a rotation of nDsbD such that Cys109 is sufficiently distant from the plane of the membrane to prevent clashes between DsbD and DsbC (Figure 4).

Specific interactions stabilizing the nDsbD-SS-cDsbD complex

Besides the interdomain disulfide bond, the nDsbD-SS-cDsbD domain interface is characterized by only a limited number of specific interactions, namely four (complex B), five (complex C), or six (complex A) interdomain hydrogen bonds (Table III). The main-chain carbonyl of Cys109 is hydrogen-bonded to the amide nitrogen of Leu510, and the amide nitrogen of Cys109 is linked to the carbonyl oxygen of Leu510. A third hydrogen bond near the active cysteines is formed by the amide nitrogen of Phe531 and by the carbonyl of Gly107. The other interdomain hydrogen bonds lie in the Cap-loop region and differ in every complex in the asymmetric unit due to conformational changes induced by crystal contacts. In complexes A and C, the side-chain amine of

Lys469 and the hydroxyl group of Tyr470 are involved in a network of hydrogen bonds with the carboxylate of Glu69. In complexes A and B, the hydroxyl group of Tyr71 also interacts with the main-chain carbonyl of Asp459, while the electron density of Tyr71 in complex B is not well defined. Overall, the number of specific contacts is rather limited relative to the size of the interface area (1301 Å², see below).

Comparison between the contact interface of nDsbD-SS-cDsbD and nDsbD-SS-DsbC

We calculated the interface areas of nDsbD-SS-cDsbD and nDsbD-SS-DsbC with the program Grasp (Nicholls *et al*, 1993) following the protocol of Janin (1997). nDsbD-SS-cDsbD has a calculated binding interface of 1301 Å², whereas nDsbD-SS-DsbC has an interface of 2045 Å² (Figure 5, Table III). This difference is caused by the second nDsbD interface in the nDsbD-SS-DsbC complex, which mediates additional noncovalent contacts between nDsbD and the second DsbC subunit.

The first interface of nDsbD-SS-DsbC is the active site interface; this interface strongly overlaps with the interface
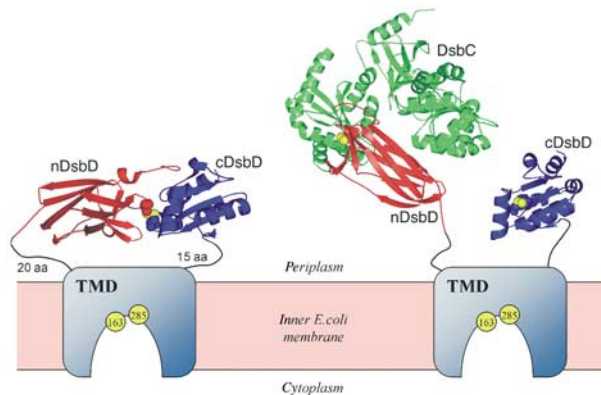

Figure 4 Electron transfer from cDsbD to DsbC via nDsbD involves large domain movements. Left: Proposed orientation of nDsbD-SS-cDsbD with respect to the transmembrane domain (TMD) in the context of full-length DsbD. Cys163 and Cys285 from the TM domain are indicted by yellow circles, and sulfur atoms of Cys109 and Cys461 are depicted by yellow spheres. The 20- and 15-residue-long linkers connecting the last structured residue of nDsbD with the first predicted TMD residue, and the last predicted TMD residue with the first structured residue of cDsbD, respectively, are indicated as black lines. Right: Model of the mixed disulfide complex between DsbD and DsbC, based on the structures of nDsbD-SS-cDsbD and nDsbD-SS-DsbC (1JZD). Disulfide exchange between nDsbD and DsbC is only possible when nDsbD and cDsbD undergo a massive domain movement.

of nDsbD-SS-cDsbD (Figure 5) and has a comparable size of 1376 Å². In fact, the nDsbD-SS-cDsbD and the nDsbD-SS-DsbC interfaces share a common area of around 90% of their surface. Similarly to the interface between nDsbD and cDsbD (4–6 interdomain hydrogen bonds), also in the nDsbD-SS-DsbC complex there is only a limited number (7) of inter-subunit hydrogen bonds (Table III). Three hydrogen bonds described for nDsbD-SS-cDsbD are located at the same position as in nDsbD-SS-DsbC. The main-chain carbonyl and the amide nitrogen of Cys109 (nDsbD) hydrogen-bond the amide nitrogen and carbonyl oxygen, respectively, of Thr182 of DsbC. The third hydrogen bond is formed by the amide nitrogen of DsbC Tyr196 and by the carbonyl of Gly107 (nDsbD).

The nDsbD-SS-DsbC complex has one residue forming intersubunit hydrogen bonds in the Cap-loop region (hydroxyl group of Tyr71 of nDsbD to the guanidinium moiety of DsbC Arg125). As mentioned above, the Cap-loop region in the nDsbD-SS-cDsbD complex is also involved in crystal contacts. In nDsbD-SS-cDsbD, the Cap-loop region exhibits a wider opening than in nDsbD-SS-DsbC.

The additional, second interface of nDsbD-SS-DsbC is stabilized by three hydrogen bonds and a specific salt bridge. Indices for planarity and shape complementarities (sc-index) were also calculated. Lower planarity and a lower sc-index are found for nDsbD-SS-cDsbD (Table III). The planarity for nDsbD-SS-cDsbD is 1.81 Å and for nDsbD-SS-DsbC 2.34 Å (first interface). Analysis of 23 optional interfaces of protein–protein complexes by Jones and Thornton (1996) updated at http://www.biochem.ucl.ac.uk/bsm/-PP/server/server_datasets.html yielded an average planarity of 2.6 Å ($\sigma = 0.6$ Å). Compared to this value, nDsbD-SS-cDsbD shows a very low planarity, whereas nDsbD-SS-DsbC shows a value that lies in the average. Comparison of these values, the wider opening of the Cap-loop region and the additional contact area in nDsbD-SS-DsbC suggest that the interaction of nDsbD with cDsbD may be less specific than that with DsbC. This is, however, most likely compensated by the high relative effective concentrations of the periplasmic domains in the context of full-length DsbD.

Large kinetic barriers guarantee the coexistence of the DsbA/B and DsbC/D redox system

We measured the rate constants of nonfunctional disulfide exchange reactions either by tryptophan fluorescence (DsbA/DsbC, DsbA/nDsbD, DsbA/cDsbD, DsbB/DsbC) or acid-quenching after different reaction times and HPLC separation of reaction products (nDsbD/DsbC, cDsbD/DsbC). Figure 6 shows that all nonfunctional disulfide exchange reactions are

Table 3 Analysis of specific interdomain contacts formed by nDsbD

	nDsbD-SS-DsbC			nDsbD-SS-cDsbD
	First interface	Second interface	Total	
Interface area (Å²)	1376 (1268)[a]	669 (654)[a]	2045 (1922)[a]	1301
Planarity (Å)[b]	2.34	1.29		1.81
Hydrogen bonds	7	3	10	4–6[d]
Salt bridges	0	1	1	0
Index of surface complementarity[c]			0.76	0.67

[a]Haebel *et al* (2002).
[b]Jones and Thornton (1997).
[c]Lawrence and Colman (1993).
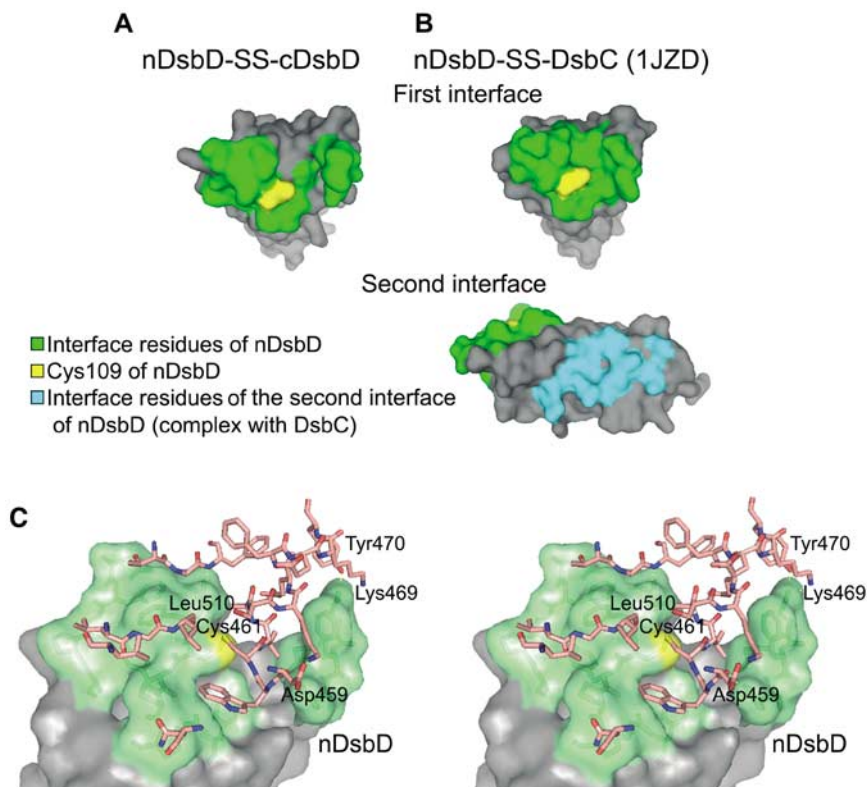[d]Depending on the respective complex in a.u.

Figure 5 Surface representations and interface analysis of the nDsbD-SS-cDsbD and nDsbD-SS-DsbC (1JZD) complexes. (**A**) Residues of nDsbD involved in the interaction with cDsbD (green). (**B**) Residues of nDsbD involved in the interaction with the first interface (green) and the second interface (cyan) of DsbC. (**C**) Details of the nDsbD-SS-cDsbD interface. Residues of nDsbD participating in the dimer interface are shown in green on the surface of the domain. The interacting residues of cDsbD appear in ball-and-stick representation in pink and atom colors.

indeed 10^3–10^7-fold slower than disulfide exchange between DsbA and DsbB, and DsbC and nDsbD, both of which have apparent second-order rate constants above $10^6 \, \mathrm{M}^{-1}\,\mathrm{s}^{-1}$ at pH 7.0. Among the nonfunctional reactions, oxidation of DsbC by quinone-depleted DsbB is fastest ($1.9 \times 10^3 \, \mathrm{M}^{-1}\,\mathrm{s}^{-1}$), albeit >1000-fold slower than oxidation of DsbA by DsbB (Figure 6). This explains that DsbC accumulates in the oxidized form in the periplasm of *dsbD* null strains (Rietsch *et al*, 1997) and indicates that DsbC may be oxidized directly by DsbB in these strains. Conversely, DsbA is also a very poor redox partner of DsbD ($k_{app} = 900 \, \mathrm{M}^{-1}\,\mathrm{s}^{-1}$), again in agreement with the predominantly reduced state of DsbA in *dsbB* deletion mutants (Kishigami *et al*, 1995). Overall, the kinetic data demonstrate that large kinetic barriers for nonfunctional disulfide exchange reactions guarantee the coexistence of the DsbA/B and DsbC/D redox systems.

Conclusions

In the present work, we have gained a complete picture on the kinetics of disulfide exchange reactions that may occur between proteins from the oxidative DsbA/B and reductive DsbC/D pathway in the *E. coli* periplasm. Overall, nonfunctional reactions between oxidoreductase components from different pathways are separated by large kinetic barriers from functional reactions, such that nonfunctional disulfide exchange is 10^3–10^7 times slower than functional electron transfer. Steric hindrance of nonfunctional interactions is likely to be the main mechanism guaranteeing the indepen-

dence of the DsbA/B and DsbC/D systems. An alternative explanation would be particularly fast, functional disulfide exchange reactions mediated through very specific side-chain contacts in the contact area between functional reaction partners. We consider this mechanism less prevalent. This is best illustrated by nDsbD, which not only interacts rapidly with cDsbD and DsbC (Katzen and Beckwith, 2000; Krupp *et al*, 2001; Collet *et al*, 2002) via its nucleophilic Cys109 thiol, but is also supposed to react rapidly with DsbG (Bessette *et al*, 1999) and CcmG (Katzen *et al*, 2002) via Cys109. It is thus difficult to conceive a single binding area around Cys109 in nDsbD that simultaneously mediates highly specific recognition of four different target proteins. Indeed, the number of specific hydrogen bonds and salt bridges in the interface between nDsbD and cDsbD relative to the total binding area of about 1300 Å^2 is very small (Table III). The same holds true for the nDsbD-SS-DsbC complex, albeit there are additional contacts to the second DsbC subunit (Table III). We thus conclude that surface complementarity to the extent that disulfide interchange between active sites can occur without steric hindrance, and a limited number of specific contacts are sufficient to mediate rapid, functional disulfide exchange between intrinsically reactive Dsb proteins. A main factor determining the intrinsic reactivities of the nucleophilic active site cysteines in proteins from the thioredoxin family is the strongly lowered pK_a value of the more N-terminal active site thiols (Nelson and Creighton, 1994). For example, the pK_a values of the nucleophilic cysteines in DsbA and DsbC are 3.4 and 4.1, respectively (Nelson and Creighton, 1994; Sun
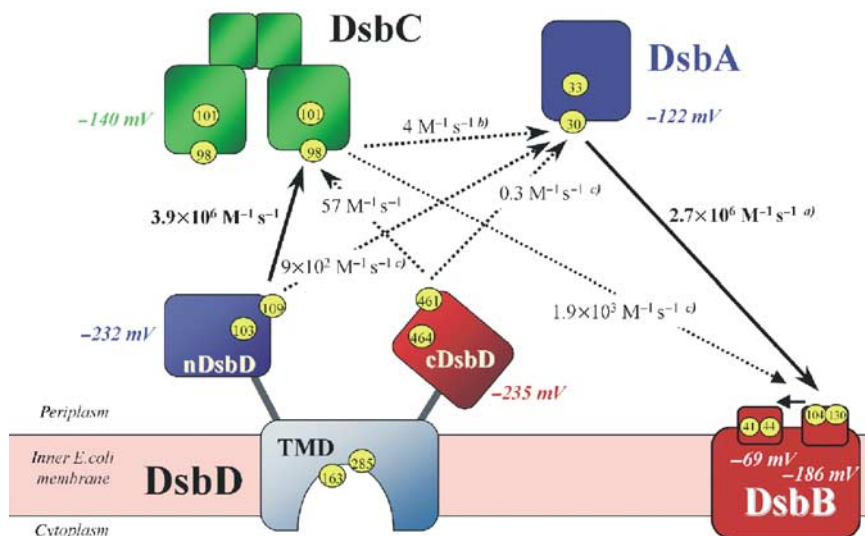
Figure 6 Large kinetic barriers separate the DsbA/B and DsbC/D redox systems. Apparent rate constants of disulfide exchange were measured at pH 7.0 and 25°C. Functional disulfide exchange reactions (bold solid arrows) have second-order rate constants above $10^6\,M^{-1}\,s^{-1}$, while nonfunctional ('forbidden') reactions (dotted arrows) are 10^3–10^7-fold slower. Arrows indicate the direction of two-electron transfer. All measured rates have errors $<30\%$. [a]Grauschopf *et al* (2003). [b]Zapun *et al* (1995) reported a value of $100\,M^{-1}\,s^{-1}$ for this reaction at pH 7.5. [c]Reactions were followed by the change in tryptophan fluorescence.

and Wang, 2000), and are sufficient to explain the high reactivity of both proteins (Szajewski and Whitesides, 1980; Grauschopf *et al*, 1995; Huber-Wunderlich and Glockshuber, 1998).

We have shown that Cys109 from nDsbD and Cys461 from cDsbD form a transient mixed disulfide bond in the reaction mechanism of DsbD, and conclude that large relative domain movements between nDsbD and cDsbD are necessary to allow electrons flow from cDsbD to DsbC. The fact that nDsbD but not cDsbD can be cleaved off proteolytically from full-length DsbD (Collet *et al*, 2002) indicates that the linker segment between nDsbD and the TM domain is more flexible than that between cDsbD and the TM domain. It may therefore well be that it is essentially nDsbD that moves away from cDsbD to allow subsequent disulfide exchange between nDsbD and DsbC, DsbG, or CcmG.

If we assume that DsbD-mediated electron transfer occurs exclusively via disulfide exchange (Chung *et al*, 2000; Katzen and Beckwith, 2000; Krupp *et al*, 2001), the last mechanistic step that remains to be elucidated will be the identification of the pair of cysteines that mediate disulfide exchange between the TM domain and cDsbD. As Cys461 is the only surface-exposed residue in cDsbD, we propose that Cys461 not only reacts with Cys109 of nDsbD, but is also capable of forming a disulfide bond with either Cys163 or Cys285 from the TM domain if this mechanism holds true. This implies additional domain movements of cDsbD relative to the TM domain. Cys163 and Cys285 are both located in the predicted TM helices 1 and 4, can form a disulfide bond that connects both helices, and have been shown to be accessible from the cytoplasmic side (Chung *et al*, 2000; Katzen and Beckwith, 2003). This has led to a model according to which the TM domain of DsbD adopts a 'funnel-like' structure, with the 'funnel' opening toward the cytoplasm when the Cys163–Cys285 disulfide is formed (Katzen and Beckwith, 2003). Direct oxidation of the Cys163–Cys285 pair by oxidized

cDsbD is thus only conceivable when a major structural rearrangement occurs in the TM domain such that the 'funnel' opens toward the periplasm when the Cys163–Cys285 disulfide is reduced by cytoplasmic thioredoxin. Alternatively, a protein-bound cofactor may assist electron transfer from the Cys163/Cys285 pair to the Cys461–Cys464 disulfide bond of cDsbD.

Materials and methods

Construction of expression plasmids
The plasmid pNDsbD for cytosolic expression of nDsbD (residues 1–143 of mature DsbD) under control of *trc*-promotor/*lac*-operator was constructed as follows. A 435-bp gene fragment encoding nDsbD was amplified by PCR from genomic DNA of the *E. coli* wild-type strain W3110 with primers N1 (5′-GGG AAT CCC ATA TGA TGG CTC AAC GCA TCT TTA CG-3′) and N2 (5′-CCC GGA TCC TTA TTG CGC GGT GGG CTG C-3′) and cloned into pDsbA3 (Hennecke *et al*, 1999) via *Nde*I and *Bam*HI.

For expression of cDsbD (residues 419–546 of mature DsbD) with C-terminal (His)$_6$ tag, a 399-bp fragment was amplified with primers C1 (5′-CTA GCT AGC CAG GAT TGG GCA TTT GGT GCG ACG C-3′) and C2 (5′-CGC GGA TCC TTA ATG GTG ATG GTG ATG GTG CGG TTG GCG ATC GCG C-3′) and cloned into pDsbA3 via *Nhe*I and *Bam*HI. In the resulting plasmid pCDsbD, the sequence encoding (His)$_6$-tagged cDsbD is fused to the DsbA signal sequence for periplasmic expression under the control of *trc*-promotor/*lac*-operator.

The Cys variants of nDsbD and cDsbD, in which one of the active site cysteines was replaced by a serine, were constructed from pNDsbD and pCDsbD using the QuikChange method (Stratagene). All constructs were verified by DNA sequencing.

Purification of nDsbD, cDsbD, DsbA, DsbB, and DsbC
All proteins were expressed in the *E. coli* BL21*Rosetta* cells (Novagene) grown in 9 l of Luria–Bertani (LB) medium containing ampicillin (100 μg/ml) at 37°C. Protein production was induced with IPTG (final concentration 100 μM) when cells had reached an optical density (OD) at 600 nm of 0.6–0.8. After further growth at 37°C for 4 h, bacteria were harvested by centrifugation.

For purification of nDsbD, cells were suspended in 5 mM Tris–HCl (pH 8.0) and disrupted (Cell Cracker). After centrifugation at

50 000 *g* for 30 min at 4°C, the supernatant was dialyzed at 4°C against 5 mM Tris–HCl (pH 8.0), and applied on Fast Flow Q Sepharose pre-equilibrated with the same buffer. Proteins were eluted with a gradient of 0 to 500 mM NaCl in 5 mM Tris–HCl (pH 8.0). Fractions containing nDsbD were pooled and mixed with ammonium sulfate to a final concentration of 1.4 M. The solution was applied to Phenyl Sepharose HP equilibrated with 1.4 M ammonium sulfate and 10 mM Tris–HCl (pH 8.0). Proteins were eluted with a gradient from 1.4 to 0 M ammonium sulfate in 10 mM Tris–HCl (pH 8.0). Fractions containing pure nDsbD were dialyzed against distilled water. The final yield of purified nDsbD was 100 mg/l bacterial culture.

For purification of cDsbD, bacteria were suspended in cold PBS buffer (20 mM sodium phosphate (pH 7.5), 150 mM NaCl) containing polymyxin B (1 mg/ml) and shaken at 4°C for 90 min. After centrifugation at 50 000 *g* for 30 min at 4°C, the supernatant was mixed with imidazole–HCl (pH 7.5) to a concentration of 10 mM and applied to an Ni-NTA Superflow column equilibrated with 10 mM imidazole–HCl and PBS (pH 7.5). Proteins were eluted with a gradient from 10 to 300 mM imidazole–HCl in PBS. Fractions containing (His)$_6$-tagged cDsbD were dialyzed against distilled water. The final yield of purified protein was 20 mg/l bacterial culture.

Cysteine variants of nDsbD and (His)$_6$-tagged cDsbD were purified according to the same protocols with comparable yields. Oxidized *E. coli* DsbA (Hennecke *et al*, 1999), oxidized *E. coli* DsbC (Maskos *et al*, 2003), and oxidized, quinone-depleted *E. coli* DsbB (Grauschopf *et al*, 2003) were purified as described.

Synthesis of nDsbD-SS-cDsbD

For preparation of nDsbD-SS-cDsbD, we first prepared the mixed disulfide between the nDsbD variant C103S and nitrothiobenzoic acid (nDsbD(C103S)-NTB). The variant C103 was produced in *E. coli* and enriched by chromatography on Fast Flow Q Sepharose as described for wild-type nDsbD. Pooled fractions (in Tris–HCl (pH 8.0)) were mixed with excess dithiobisnitrobenzoic acid (DTNB) (final concentration 10 mM) and incubated at 25°C for 15 min. After addition of ammonium sulfate to a concentration of 1.2 M, the solution was applied to Phenyl Sepharose HP equilibrated with 1.2 M ammonium sulfate and 10 mM Tris–HCl (pH 8.0). The mixed disulfide was eluted with a gradient from 1.2 to 1 M ammonium sulfate. Fractions containing nDsbD(C103S)-NTB were pooled and dialyzed against PBS (pH 7.5). The (His)$_6$-tagged variant C464S of cDsbD was purified from the periplasmic extract as described for (His)$_6$-tagged wild-type cDsbD, and also dialyzed against PBS (pH 7.5).

Purified nDsbD(C103S)-NTB and cDsbD(C464S) were then mixed at equimolar concentrations (30 μM each), incubated in PBS for 30 min at 25°C, and applied to an Ni-NTA Superflow column equilibrated with PBS (pH 7.5). The column was washed with PBS and 10 mM imidazole–HCl (pH 7.5), and the nDsbD(C103S)-cDsbD(C464S) mixed disulfide (nDsbD-SS-cDsbD) was eluted with a gradient from 10 to 70 mM imidazole–HCl. Fractions containing the mixed disulfide and small amounts of cDsbD were concentrated and subjected to gel filtration on a Superdex 75 16/60 column in 100 mM sodium phosphate and 500 mM NaCl (pH 7.0). Fractions containing the pure complex were dialyzed against distilled water and concentrated.

Protein concentrations

Protein concentrations were determined according to the molar extinction coefficients at 280 nm, using values of 20 000 and 8300 M^{-1} cm^{-1} for native nDsbD and native cDsbD, respectively. For oxidized DsbA, DsbC, and DsbB, extinction coefficients of 23 250, 16 200, and 47 750 M^{-1} cm^{-1} were used, respectively. Reduced proteins were prepared by reduction with a 1000-fold molar excess of DTT at pH 8.0, followed by gel filtration in 0.1 mM EDTA. Free thiol groups in reduced proteins were quantified by Ellman's assay (Ellman, 1959) using $\varepsilon_{412\,nm} = 13\,600$ M^{-1} cm^{-1} per free thiol group.

HPLC analysis of disulfide exchange kinetics

Disulfide exchange reactions between Dsb proteins were performed at 25°C and initial protein concentrations between 0.25 and 75 μM under second-order or pseudo-first-order conditions in 100 mM sodium phosphate and 0.1 mM EDTA (pH 7.0). Samples were removed after different incubation times, and the reactions were rapidly quenched by addition of 0.4 volumes of 30% (w/v) formic acid (final pH < 2). Reaction products were separated with an Agilent 1100 HPLC instrument equipped with a diode array detection system and a C$_{18}$ reverse-phase column (Agilent Zorbax 300 SB, 5 μM, 2.1 × 150 mm). Proteins were eluted at 55°C with a linear gradient of H$_2$O/0.1% TFA and acetonitirile/0.07% TFA, and detected by their absorbance at 220 and 280 nm.

Fluorescence measurements

Disulfide exchange between DsbC$_{red}$ and DsbB$_{ox}$, and between nDsbD$_{red}$ (or cDsbD$_{red}$) and DsbA$_{ox}$ was followed by the change in tryptophan fluorescence at 330 nm (excitation at 280 nm) in 100 mM sodium phosphate and 0.1 mM EDTA (pH 7.0). Initial protein concentrations varied between 5 and 50 μM for the individual reactions.

Redox equilibria

For determination of equilibrium constants (K_{eq}) between Dsb proteins and glutathione or DTT (cf. Grauschopf *et al*, 2003 and references cited therein), the redox state of the respective protein at different [GSH]^2/[GSSG] or DTT$_{ox}$/DTT$_{red}$ ratios was determined. Proteins were incubated for 16 h at 25°C in 100 mM sodium phosphate and 0.1 mM EDTA (pH 7.0) containing the respective thiol-disulfide mixtures. In the case of nDsbD, the fraction of reduced protein was quantified by Ellman's assay after removal of excess DTT through gel filtration. In the case of cDsbD and DsbC, the oxidized and reduced forms of the protein were separated and quantified by reverse-phase HPLC after acid quenching. cDsbD and nDsbD were equilibrated with DTT$_{ox}$/DTT$_{red}$ mixtures, while DsbC was incubated with glutathione redox buffers. To exclude air oxidation, all buffers were degassed and flushed with argon. Standard redox potentials (E_o') were calculated by the Nernst equation ($E_o'_{protein} = E_o'_{reference} - (RT/2F) \ln K_{eq}$), using E_o' values of −0.240 and −0.307 V for the redox potentials of glutathione and DTT$_{ox}$/DTT$_{red}$, respectively (Rost and Rapoport, 1964; Rothwarf and Scheraga, 1992).

Crystallization and structure determination

Purified disulfide-linked nDsbD-SS-cDsbD complex in distilled water was concentrated to 40 mg/ml. The sitting drop vapor diffusion method was used for producing crystals. A measure of 1 μl of protein solution was mixed with 1 μl of mother liquor solution (0.1 M sodium acetate (pH 4.5), 0.8 M sodium formate, 25% PEG 2K MME). Plate-like crystals grew at 4°C within a week to maximum dimensions of 130 × 500 × 30 μm. Crystals were cryo-protected by adding 15% ethylene glycol to the mother liquor solution and directly frozen in the nitrogen gas stream. Diffraction data were collected at 98.2 K on beamline X06SA at the Swiss Light Source (Paul Scherrer Institut Villigen, Switzerland) using a MAR CCD image plate at a wavelength of 0.7514 Å. The short wavelength was chosen to reduce synchrotron radiation damage to the disulfide bridge (Schlichting *et al*, 2000). Data were processed with DENZO and SCALEPACK (Otwinowski and Minor, 1997) to 2.85 Å. nDsbD-SS-cDsbD crystals belong to space group C2 with $a = 188.5$ Å, $b = 52.6$ Å, $c = 107.9$ Å, and $\beta = 100.4°$, and contain three molecules per asymmetric unit (Table II).

The structure of nDsbD-SS-cDsbD was solved by molecular replacement with AMoRe (Navaza, 1994) using the structure of nDsbD from the nDsbD-SS-DsbC structure (PDB entry 1JZD; Haebel *et al*, 2002) and a high-resolution structure of cDsbD (G Capitani and Ch U Stirnimann, unpublished data) as search models, against 12–4 Å data. Solutions for two complexes could be found using AMoRe against the data processed in C2. This corresponds to four solutions against data processed in P1. These four P1 solutions were refined in CNS (Brünger *et al*, 1998) to an *R*-factor of 0.418 and a free *R*-factor of 0.426. Nine cycles of water picking (with ARP/wARP-like picking parameters) and density modification in CNS lead to a much improved map, which was skeletonized with MAPMAN (Kleywegt and Jones, 1996). The waters introduced in the previous phase improvement step were deleted. The structure refined to an *R*-factor of 0.308 and a free *R*-factor of 0.348 after having fitted the fifth and sixth complexes to the skeleton and to the density by hand using the program O (Jones *et al*, 1991). Molecular replacement in AMoRe worked now in C2 by picking the three corresponding P1 solutions. The nDsbD-SS-cDsbD structure was iteratively rebuilt in O and refined in CNS using NCS restraints to an *R*-factor of 0.224 and a free *R*-factor of 0.284 in space group C2

(Table II). The coordinates and structure factors of nDsbD-SS-cDsbD were deposited with the Protein Data Bank (http://www.rcsb.org/pdb/) with entry code 1SE1.

The stereochemistry of the nDsbD-SS-cDsbD structure was checked with WHAT_CHECK (Hooft *et al*, 1996) and PROCHECK (Laskowski *et al*, 1993). All figures were prepared with PyMOL (http://www.pymol.org; DeLano, 2002) except for Figure 1B, for which SwissPDB Viewer was used (http://www.expasy.org/spdbv; Guex and Peitsch, 1997). The interface areas of the nDsbD-SS-cDsbD and nDsbD-SS-DsbC complexes were calculated with the program Grasp (Nicholls *et al*, 1993). The shape complementarity of the interfaces of nDsbD-SS-cDsbD and nDsbD-SS-DsbC was calculated with the CCP4 program SC (Lawrence and Colman, 1993).

References

Andersen CL, Matthey-Dupraz A, Missiakas D, Raina S (1997) A new *Escherichia coli* gene, dsbG, encodes a periplasmic protein involved in disulphide bond formation, required for recycling DsbA/DsbB and DsbC redox proteins. *Mol Microbiol* **26:** 121–132

Bader M, Muse W, Ballou DP, Gassner C, Bardwell JC (1999) Oxidative protein folding is driven by the electron transport system. *Cell* **98:** 217–227

Bader MW, Xie T, Yu CA, Bardwell JC (2000) Disulfide bonds are generated by quinone reduction. *J Biol Chem* **275:** 26082–26088

Bardwell JC, Lee JO, Jander G, Martin N, Belin D, Beckwith J (1993) A pathway for disulfide bond formation *in vivo*. *Proc Natl Acad Sci USA* **90:** 1038–1042

Bessette PH, Cotto JJ, Gilbert HF, Georgiou G (1999) *In vivo* and *in vitro* function of the *Escherichia coli* periplasmic cysteine oxidor-eductase DsbG. *J Biol Chem* **274:** 7784–7792

Brünger AT, Adams PD, Clore GM, DeLano WL, Gros P, Grosse-Kunstleve RW, Jiang JS, Kuszewski J, Nilges M, Pannu NS, Read RJ, Rice LM, Simonson T, Warren GL (1998) Crystallography & NMR system: a new software suite for macromolecular structure determination. *Acta Crystallogr D* **54:** 905–921

Chung J, Chen T, Missiakas D (2000) Transfer of electrons across the cytoplasmic membrane by DsbD, a membrane protein involved in thiol-disulphide exchange and protein folding in the bacterial periplasm. *Mol Microbiol* **35:** 1099–1109

Collet JF, Bardwell JC (2002) Oxidative protein folding in bacteria. *Mol Microbiol* **44:** 1–8

Collet JF, Riemer J, Bader MW, Bardwell JC (2002) Reconstitution of a disulfide isomerization system. *J Biol Chem* **277:** 26886–26892

Dailey FE, Berg HC (1993) Mutants in disulfide bond formation that disrupt flagellar assembly in *Escherichia coli*. *Proc Natl Acad Sci USA* **90:** 1043–1047

Darby NJ, Creighton TE (1995) Catalytic mechanism of DsbA and its comparison with that of protein disulfide isomerase. *Biochemistry* **34:** 3576–3587

DeLano WL (2002) *The PyMol Molecular Graphics System*. San Carlos, CA, USA: DeLano Scientific

Ellman GL (1959) Tissue sulfhydryl groups. *Arch Biochem Biophys* **82:** 70–77

Goldstone D, Haebel PW, Katzen F, Bader MW, Bardwell JC, Beckwith J, Metcalf P (2001) DsbC activation by the N-terminal domain of DsbD. *Proc Natl Acad Sci USA* **98:** 9551–9556

Gordon EH, Page MD, Willis AC, Ferguson SJ (2000) *Escherichia coli* DipZ: anatomy of a transmembrane protein disulphide reductase in which three pairs of cysteine residues, one in each of three domains, contribute differentially to function. *Mol Microbiol* **35:** 1360–1374

Goulding CW, Sawaya MR, Parseghian A, Lim V, Eisenberg D, Missiakas D (2002) Thiol-disulfide exchange in an immunoglo-bulin-like fold: structure of the N-terminal domain of DsbD. *Biochemistry* **41:** 6920–6927

Grauschopf U, Fritz A, Glockshuber R (2003) Mechanism of the electron transfer catalyst DsbB from *Escherichia coli*. *EMBO J* **22:** 3503–3513

Grauschopf U, Winther JR, Korber P, Zander T, Dallinger P, Bardwell JC (1995) Why is DsbA such an oxidizing disulfide catalyst? *Cell* **83:** 947–955

Guex N, Peitsch MC (1997) SWISS-MODEL and the Swiss-PdbViewer: an environment for comparative protein modeling. *Electrophoresis* **18:** 2714–2723

Haebel PW, Goldstone D, Katzen F, Beckwith J, Metcalf P (2002) The disulfide bond isomerase DsbC is activated by an immuno-globulin-fold thiol oxidoreductase: crystal structure of the DsbC–DsbDalpha complex. *EMBO J* **21:** 4774–4784

Hennecke J, Sebbel P, Glockshuber R (1999) Random circular permutation of DsbA reveals segments that are essential for protein folding and stability. *J Mol Biol* **286:** 1197–1215

Hiniker A, Bardwell JC (2003) Disulfide bond isomerization in prokaryotes. *Biochemistry* **42:** 1179–1185

Hooft RW, Vriend G, Sander C, Abola EE (1996) Errors in protein structures. *Nature* **381:** 272

Huber-Wunderlich M, Glockshuber R (1998) A single dipeptide sequence modulates the redox properties of a whole enzyme family. *Fold Des* **3:** 161–171

Janin J (1997) Specific versus non-specific contacts in protein crystals. *Nat Struct Biol* **4:** 973–974

Jones S, Thornton JM (1996) Principles of protein–protein inter-actions. *Proc Natl Acad Sci USA* **93:** 13–20

Jones S, Thornton JM (1997) Prediction of protein–protein inter-action sites using patch analysis. *J Mol Biol* **272:** 133–143

Jones TA, Zou J-Y, Cowan SW, Kjeldgaard M (1991) Improved methods for building protein models in electron density maps and the location of errors in these models. *Acta Crystallogr A* **47:** 110–119

Katzen F, Beckwith J (2000) Transmembrane electron transfer by the membrane protein DsbD occurs via a disulfide bond cascade. *Cell* **103:** 769–779

Katzen F, Beckwith J (2003) Role and location of the unusual redox-active cysteines in the hydrophobic domain of the transmem-brane electron transporter DsbD. *Proc Natl Acad Sci USA* **100:** 10471–10476

Katzen F, Deshmukh M, Daldal F, Beckwith J (2002) Evolutionary domain fusion expanded the substrate specificity of the trans-membrane electron transporter DsbD. *EMBO J* **21:** 3960–3969

Kim JH, Kim SJ, Jeong DG, Son JH, Ryu SE (2003) Crystal structure of DsbDgamma reveals the mechanism of redox potential shift and substrate specificity. *FEBS Lett* **543:** 164–169

Kishigami S, Akiyama Y, Ito K (1995) Redox states of DsbA in the periplasm of *Escherichia coli*. *FEBS Lett* **364:** 55–58

Kleywegt GJ, Jones TA (1996) xdlMAPMAN and xdlDATAMAN—programs for reformatting, analysis and manipulation of bioma-cromolecular electron-density maps and reflection data sets. *Acta Crystallogr D* **52:** 826–828

Kobayashi T, Ito K (1999) Respiratory chain strongly oxidizes the CXXC motif of DsbB in the *Escherichia coli* disulfide bond forma-tion pathway. *EMBO J* **18:** 1192–1198

Krupp R, Chan C, Missiakas D (2001) DsbD-catalyzed transport of electrons across the membrane of *Escherichia coli*. *J Biol Chem* **276:** 3696–3701

Laskowski RA, MacArthur MW, Moss DS, Thornton JM (1993) PROCHECK: a program to check the stereochemical quality of protein structure. *J Appl Crystallogr* **26:** 283–291

Lawrence MC, Colman PM (1993) Shape complementarity at pro-tein/protein interfaces. *J Mol Biol* **234:** 946–950

Maskos K, Huber-Wunderlich M, Glockshuber R (2003) DsbA and DsbC-catalyzed oxidative folding of proteins with complex disulfide bridge patterns *in vitro* and *in vivo*. *J Mol Biol* **325:** 495–513

McCarthy AA, Haebel PW, Torronen A, Rybin V, Baker EN, Metcalf P (2000) Crystal structure of the protein disulfide bond isomerase, DsbC, from *Escherichia coli*. *Nat Struct Biol* **7:** 196–199

Missiakas D, Georgopoulos C, Raina S (1994) The *Escherichia coli* dsbC (xprA) gene encodes a periplasmic protein involved in disulfide bond formation. *EMBO J* **13:** 2013–2020

Navaza J (1994) AMoRe: an automated package for molecular replacement. *Acta Crystallogr A* **50:** 157–163

Nelson JW, Creighton TE (1994) Reactivity and ionization of the active site cysteine residues of DsbA, a protein required for disulfide bond formation *in vivo*. *Biochemistry* **33:** 5974–5983

Nicholls A, Bharadwaj R, Honig B (1993) GRASP graphical representation and analysis of surface properties. *Biophys J* **64:** A166

Otwinowski Z, Minor W (1997) Processing of X-ray diffraction data collected in oscillation mode. *Methods Enzymol* **276:** 307–328

Reid E, Cole J, Eaves DJ (2001) The *Escherichia coli* CcmG protein fulfils a specific role in cytochrome *c* assembly. *Biochem J* **355:** 51–58

Rietsch A, Bessette P, Georgiou G, Beckwith J (1997) Reduction of the periplasmic disulfide bond isomerase, DsbC, occurs by passage of electrons from cytoplasmic thioredoxin. *J Bacteriol* **179:** 6602–6608

Ritz D, Beckwith J (2001) Roles of thiol-redox pathways in bacteria. *Annu Rev Microbiol* **55:** 21–48

Rost J, Rapoport S (1964) Reduction-potential of glutathione. *Nature* **201:** 185

Rothwarf DM, Scheraga HA (1992) Equilibrium and kinetic constants for the thiol-disulfide interchange reaction between glutathione and dithiothreitol. *Proc Natl Acad Sci USA* **89:** 7944–7948

Schlichting I, Berendzen J, Chu K, Stock AM, Maves SA, Benson DE, Sweet RM, Ringe D, Petsko GA, Sligar SG (2000) The catalytic pathway of cytochrome p450cam at atomic resolution. *Science* **287:** 1615–1622

Stewart EJ, Katzen F, Beckwith J (1999) Six conserved cysteines of the membrane protein DsbD are required for the transfer of electrons from the cytoplasm to the periplasm of *Escherichia coli*. *EMBO J* **18:** 5963–5971

Sun XX, Wang CC (2000) The N-terminal sequence (residues 1–65) is essential for dimerization, activities, and peptide binding of *Escherichia coli* DsbC. *J Biol Chem* **275:** 22743–22749

Szajewski RP, Whitesides GM (1980) Rate constants and equilibrium constants of thiol-disulfide interchange reactions involving oxidized glutathione. *J Am Chem Soc* **102:** 2011–2026

van Straaten M, Missiakas D, Raina S, Darby NJ (1998) The functional properties of DsbG, a thiol-disulfide oxidoreductase from the periplasm of *Escherichia coli*. *FEBS Lett* **428:** 255–258

Wunderlich M, Otto A, Seckler R, Glockshuber R (1993) Bacterial protein disulfide isomerase: efficient catalysis of oxidative protein folding at acidic pH. *Biochemistry* **32:** 12251–12256

Zapun A, Creighton TE (1994) Effects of DsbA on the disulfide folding of bovine pancreatic trypsin inhibitor and alpha-lactalbumin. *Biochemistry* **33:** 5202–5211

Zapun A, Missiakas D, Raina S, Creighton TE (1995) Structural and functional characterization of DsbC, a protein involved in disulfide bond formation in *Escherichia coli*. *Biochemistry* **34:** 5075–5089